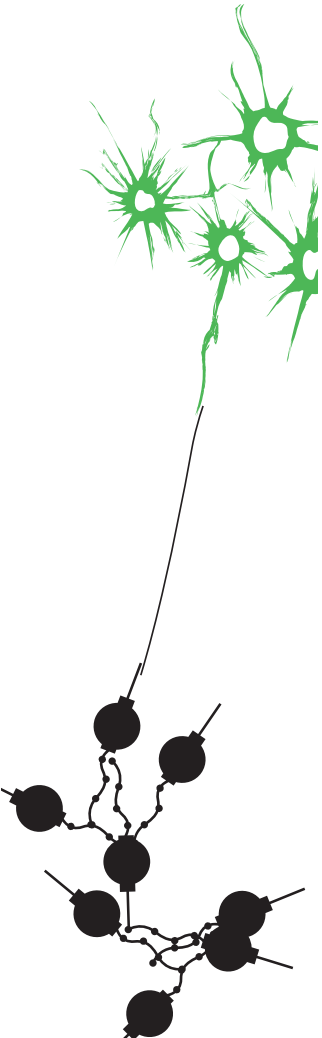

RAM ROBOTICS AND MECHATRONICS

DEVELOPMENT OF INSTRUMENTED, FFF 3D PRINTED, PESSARY RINGS TO QUANTIFY DEFORMATIONS

L.S. (Larissa) van Deinse

BSC ASSIGNMENT

Committee:
prof. dr. ir. G.J.M. Krijnen
ir. D. Kosmas
dr. ir. J. Rouwkema

February, 2023

005RaM2023
Robotics and Mechatronics
EEMCS
University of Twente
P.O. Box 217
7500 AE Enschede
The Netherlands

UNIVERSITY OF TWENTE. | TECHMED CENTRE UNIVERSITY OF TWENTE. | DIGITAL SOCIETY INSTITUTE

Summary

This bachelor assignment concerns the development of 3D printed pessary rings to sense mechanical deformations. Instead of using the more complicated torus shape, it is simplified to a cylinder. Different models are examined to deduce the locations of highest stress during compression of the cross-section, a deformation that is know to be present in a successfully implemented pessary. A decision is made between a piezoresistive readout and a capacitive one. The piezoresistive configuration was chosen due to the simpler implementation. Two designs are fabricated and tested, one with multiple conductive PI-ETPU wires running along the length of the cylinder, and one with two conductive PI-ETPU plates going from the center to the outside of the cylinder made from X60 TPU. The results indicate that the sensors can indeed respond to the compression. A peculiar shape was observed in the responses that was also observed in previous research. Possible causes are speculated and recommendations are made for further research.

Acknowledgements

This report is the result of my Bachelor Assignment for Advanced Technology. In 11 weeks I got to learn a lot about the world of 3D printing and all the new and interesting applications it has.

Even though I had a rocky start, the support I received helped me get through it all with loads of new abilities and experiences. Gijs Krijnen first introduced me to the assignments and helped me find one that fit my interests. He also provided valuable input along the way and new insights to give direction to my research. Thanks for all the help!

Of course Dimitris Kosmas was an integral part of this journey as well. As my daily supervisor he was always available to help me overcome obstacles, guide me in the right direction and provide some extra information on the topic. No matter how small the problem, I could count on his help. And despite the busy final weeks, he still found time to provide me with valuable feedback on my report, up until hours before finalizing it.

I also couldn't have done it without the help and feedback from the Nature Inspired Fabrication and Transduction (NIFTy) group. Together they posses a wealth of knowledge on 3D printing, and so much more, that no one person could acquire. The bi-weekly meetings would always help me step forward, and every one of them would help me where they could.

I'd like to thank Jeroen Rouwkerma for being part of my examination committee.

Besides any academic help, there are other forms of support that helped me through my assignment. Without the graduation support group I would not have had enough discipline to get where I am now. And without my parents and friends, some new, some old, this would not have been the pleasant experience it was.

Larissa February 2023

List of Abbreviations

ABS Acrylonitrile Butadiene Styrene.

DIW Direct-Ink-Writing.

FDM Fused Deposition Modeling.

FFF Fused Filament Fabrication.

NIFTy Nature Inspired Fabrication and Transduction.

PETG Polyethylene Terephthalate Glycol.

PLA Polyactic Acid.

POP Pelvic Organ Prolapse.

TPE Thermoplastic Elastomer.

TPU Thermoplastic Polyurethane.

Contents

1 Introduction **1**
1.1 Context . . . 1
1.2 Fabrication . . . 1
1.3 Objectives . . . 3
1.4 Report structure . . . 3

2 Design and fabrication **4**
2.1 Introduction . . . 4
2.2 Simplification . . . 4
2.3 Deformation . . . 4
2.4 Sensing principle . . . 5
2.5 Sensor placement . . . 6
2.6 Visualization . . . 7
2.7 Fabrication . . . 7
2.8 Conclusion . . . 9

3 Measurements **10**
3.1 Introduction . . . 10
3.2 Measurement setup . . . 10
3.3 Measurement procedure . . . 13
3.4 Adaptations . . . 13
3.5 Results . . . 14
3.6 Conclusion . . . 21

4 Conclusions and recommendations **22**

A Settings **23**

B Experimental results **24**
B.1 Wire sensor response . . . 24
B.2 Loose sensor response . . . 25
B.3 Resistances of plate sensor . . . 26

C MatLab scripts **27**
C.1 Main script for reading the DEWE . . . 27
C.2 Script for controlling the SMAC actuator . . . 29

Bibliography **32**

1 Introduction

1.1 Context

After having children, about 5–10 % of women [1] suffer from a Pelvic Organ Prolapse (POP) that negatively affects their quality of life. The first possible treatment is using a pessary (see figure 1.1 for some examples), a flexible structure that is inserted into the vagina for support. At first the pessaries used were arbitrary objects such as half a pomegranate [2, 3], and only later were they made with the intention to to function as a pessary. Nowadays there are specialized pessaries to be used against vaginal wind (also known as vaginal flatulence), neonatal prolapse, prolapse during pregnancy and voiding dysfunction [3]. Unfortunately this treatment for pelvic organ prolapse is unsuccessful 32–40 % [1] of the time for usually unknown reasons. Hence it is suspected that a pessary that can also act as an electrical sensor, measuring the mechanical properties, would help towards identifying the problem. Being able to accurately measure the position, orientation, deformation and interaction forces of the pessary might provide insight into the underlying phenomena and allow improvement of the pessary treatment success rate.

Figure 1.1: Examples of silicon pessaries [4].

1.2 Fabrication

Fabrication of the pessaries is one of the points of interest, and one of the newer approaches uses a 3D printer. The 3D printing of sensors is less time consuming than more traditional methods, like moulding or machining, and can have lower fabrication costs [5] with high customization at low quantity [6], while the techniques are only improving as time goes on [7]. Aside from pessaries, 3D printing of sensors has already shown promising results, as in the fabrication of a thrust force sensor [8], the creation of smart tires providing information on the road [9], monitor bodily functions (like flexible EMG for muscle contractions), integration with prosthetics [10, 11] or even directly printing on top of an active organ [12].

1.2.1 Fused Filament Fabrication

One of the most prevalent methods is Fused Filament Fabrication (FFF), also known as Fused Deposition Modeling (FDM), due to its low material cost and high accessibility [7]. In FFF, a filament is extruded out of a heated nozzle onto a build platform typically by one or two driving gears, producing the object layer by layer. A schematic of a direct drive (when the extruder is mounted on the hotend) nozzle can be found in figure 1.2.

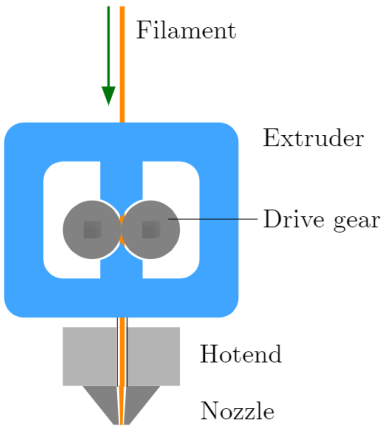

Figure 1.2: Example of a nozzle used for FFF printing [13].

The most often used filaments, Acrylonitrile Butadiene Styrene (ABS), Polyethylene Terephthalate Glycol (PETG) and Polyactic Acid (PLA), are stiff plastics which are unsuitable when the deformations are large or when soft structures are required, like often in the human body. When greater deformations are required, something pessaries only experience during insertion, more flexible filaments are used, like Thermoplastic Elastomer (TPE) and Thermoplastic Polyurethane (TPU). It could also be possible to mix these filaments for custom mechanical and electrical properties (Young's modulus, conductivity, gauge factor) [9]. Unfortunately the softer filaments might result in problems during extrusion such as kinking and buckling. However, these issues can be relieved by optimizing the print parameters and utilizing slightly different extrusion techniques (two driving gears instead of one for example) [9]. A majority of the sensors in the mentioned literature utilize the piezoresistivity of a conductive material, where deformations result in a measurable change in resistivity. When printing the sensors, one of the factors influencing the electrical and mechanical properties is the extrusion temperature. This can be controlled to improve the consistency in behaviour of the sensors. One study found an optimal procedure where over 80 % of the tested sensors exhibited consistent piezoresistive behaviour [14].

1.2.2 Injection

Other researchers focus on injecting sensing material into channels [10, 15]. The advantage of this is a reduced amount of manufacturing steps with a decreased possibility of a short circuit. A drawback is that long channels can cause undefined problems during injection, so Vatani et al. attempted to print two structures, and combine them later, but this method turned out to be less reliable. The recommended option to print a tactile sensor is to combine the previous methods to overcome the long channels and the requirement to pause the printing halfway, while still resulting in a reliable sensor [15].

1.2.3 Direct-Ink-Writing

The next method is Direct-Ink-Writing (DIW), where liquid (possibly conductive) inks are deposited on a (3D printed) object. One of the main obstacles in this approach is that the available inks need to be sintered at lower temperatures than optimal in order to not damage the most common materials used for 3D printed objects. A proposed solution is to transfer the printed sensors onto a 3D printed object afterward, allowing for more flexibility in the production [16].

1.2.4 3D printing sensors

Several 3D printing techniques are suitable for the creation of sensors. A common drawback for 3D printed objects is that they usually have a rough surface that requires additional processing to be suitable for use with conductive inks [16]. It is still possible to use conductive filaments with 3D printed objects, however, as has been done by the NIFTy group in the past. The parallel lines of the deposited filament (traxels) printed on top of each other make the object anisotropic due to different contact areas and gaps between the filament and different layers. Current research suggests that more investigation into traxel deposition is required to combat this complication [10]. In addition the process is very dependent on the type of 3D printer, the printing method and the settings and specifications of the printer [5]. Since this research is relatively new, there is also a lack of information on the durability of these sensors, and some methods make use of nanoparticles, which can be a safety hazard [5]. Although there is a lot of ongoing research about 3D printing sensors and about pessaries, there are still a few prevalent obstacles. These include 3D printed objects having a rough unsuitable surface, hard filaments (ABS, PLA, PETG) being unsuitable for large deformations and soft filaments (TPE, TPU) causing problems during extrusion, and the current possible sensors lacking reliability in the response [15].

1.3 Objectives

The main objective of this work is to investigate how a 3D printed structure resembling a pessary can sense mechanical deformations by integrating a sensing structure using conductive materials. It can be sub-categorized in the following questions:

- How does a model describe the deformations of a torus shape under radial loading?
- Which sensing principle is the most suitable for this application?
- What is the best configuration and location to integrate the sensors by means of FFF printing?

The employed fabrication technique is Fused Filament Fabrication using a Diabase H-series 3D printer, and the materials will be X60 [17] TPU and PI-ETPU [18] as the non-conductive and conductive material respectively. How the sensor can effectively recognize deformations will be determined by performing experiments where the structures are compressed using a SMAC actuator and measuring the response and relative resistance change.

1.4 Report structure

In order to answer the research questions, this report will start by looking at possible models and simplifications in chapter 2. The findings will then be used to produce two separate sensor designs that can be fabricated using a 3D printer. Next the experimental setup will be described, followed by the measurement procedure and results in chapter 3. Lastly will be the conclusion and discussion, which will also include some suggestions for further research.

2 Design and fabrication

2.1 Introduction

To decide on the sensor placement, insight can be gained from an analytical model that provides the relation between the quantities of interest. In this case these quantities are the deformation, strain and stress. To make the analysis easier, simplifications are often necessary, and this chapter will describe which simplifications where made, which type of deformations will be the focus and how the findings were implemented into making a sensor design.

2.2 Simplification

There are existing models that focus on the complete picture of a torus, or a similar O-ring [19]. A majority of these, however, focus on experimental results, finite element analysis [20] or on thin-walled tori, the last of which deviates too much from the pessary situation. The few analytical analyses of thin-walled tori [21, 22] are too complex for this research. Further development of pessaries capable of sensing could make use of these models to get more accurate results.

Instead of trying to work around the torus shape, it was decided to change it to a cylinder shape. When considering a small slice (the green or red circles in figure 2.1) with a circular shape, it was assumed that as long as the boundaries of the cylinder can be ignored it will give a sufficient approximation for this research. Another option to simplify the situation would be to approximate the torus as a beam (following from the approximation of a cylinder), but this introduces even more inaccuracies. As a start the hard edges present in a beam behave very differently then a circular structure when under pressure. Additionally the edges take away some of the symmetry, and deformation will change depending on the direction compared to the beam. A cylinder does still possess the cylindrical symmetry that the cross section of a torus has as well.

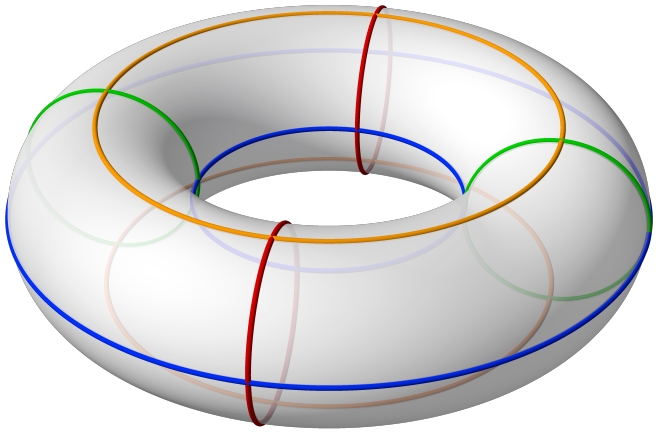

Figure 2.1: A torus shape with reference circles [23].

2.3 Deformation

The next important decision to make is which type of deformation will be the focus. This research will focus on measuring the presence of any type of deformation, albeit a main one still has to be chosen for the testing and sensor placement. Some obvious examples consist of twisting the ring, folding it (which mostly happens during insertion), compressing the entire ring and applying pressure on the cross-section (by 'pinching' the torus in figure 2.1 on one of the red or green rings). Looking at the results of successful pessary implementations [24, 25]

from a satisfied patient in figure 2.2a reveals that compression of the cross-section is a realistic deformation for successfully implemented pessaries. Although this cannot immediately be concluded from another satisfied patient in figure 2.2b, it does indicate that the pessary is not completely folded. Other deformations could still be present as these are only two dimensional slices of the implementation. Due to the simplification of a torus to a cylinder, applying pressure on the cross-section is a simple but realistic deformation to focus on.

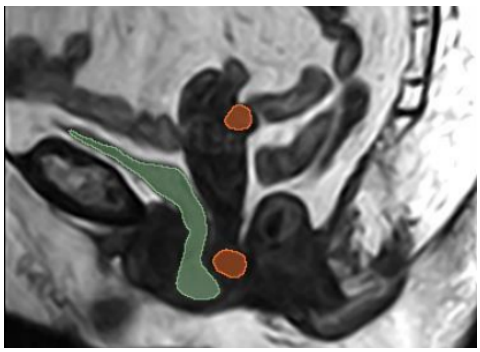

(a) Implementation of a pessary in orange, and bladder in green [24].

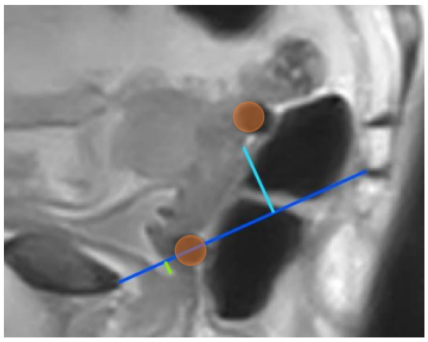

(b) Successfully implemented pessary in orange [25].

Figure 2.2: Successfully implemented pessaries of satisfied patients.

2.4 Sensing principle

By 3D printing conductive materials, the two most employed methods of constructing an element capable of sensing deformations is by using piezoresistivity or by creating a capacitive structure. Both have their advantages and disadvantages, and choosing a suitable structure is important for the success of the sensor.

2.4.1 Piezoresistive

When a material is piezoresistive, the resistance will change as a result of mechanical strains. By careful placement of a piezoresistive material, it is possible to detect and quantify a deformation by measuring the resistance change when force is applied. Some of the advantages this principle provides are the relatively simple structure that is easy to implement and read out and that it is less susceptible to electromagnetic interference from outside, with a fast response [26]. In addition, for piezoresistive filaments, the sensitivity is high but the costs are low [13].

One of the disadvantages is that (piezo)resistivity is more temperature dependent [26]. Another issue that will be relevant is the non-linearity when the strains are large [13] and the hysteresis that many (3D printed) plastic materials exhibit. There are possibilities to remedy this, however, by using differential measurements [27], but this does complicate the design. The highest strains for this application will be during insertion, a process not of interest for the effectiveness of the pessary. The actual compression is expected to be relatively small, so that the non-linearity can be largely ignored for this initial research. Further research could take this into account to design more complex and accurate sensors.

2.4.2 Capacitive

Another commonly used method is by measuring the change in capacitance between two electrodes, e.g. plates, when the distance or overlap is altered. Changing either the distance between the plates or the area of overlap can create a measurable difference in the capacitance of the structure that can be linked to applied force in many cases. Some advantages it has over piezoresistive materials is that it has a low thermal drift [13, 26, 28], high resolution and good

noise performance [26]. Most importantly, non-linearity does not majorly influence the results compared to the piezoresistive options [13].

There are some drawbacks that have to be considered as well. A capacitive readout is more complex to read out and produce, and the robustness is limited [26]. The main obstacle however is that proper shielding is required because parasitic capacitances can easily influence the system [13, 26].

2.4.3 Final decision

The chosen method utilizes the piezoresistive properties of the filament to detect deformation. The main reasoning behind this choice is the simpler implementation compared to a capacitive readout, and the ease with which multiple sensors can be added. Due to small scale of the structure, having a third plate to act as capacitance greatly complicates the system, with multiple extra capacitances to take into account, and shielding will be quite a challenge for this application. Hence a piezoresistive setup will be used. However, there is one crucial difference with the normal application of piezoresistive elements, namely the sensing direction. Most piezo sensors measure the resistance change in the direction of the deformation (lengthening or shortening of a strip), whereas this case will measure the resistance perpendicular to the deformation. The area of the cross-section will change, changing the resistance, instead of the length substantially changing.

2.5 Sensor placement

The most straightforward way to implement the strain gauges is by embedding 2 conductive plates in the cylinder that will act as strain gauges. They will be most effective at the point of the greatest stress. In the case of this deformation this is also the point of the greatest deformation. It follows from the stress profile (see figure 2.3) created by Asghar Aryanfar et al. [29] that the greatest stress during radial loading is along the edges.

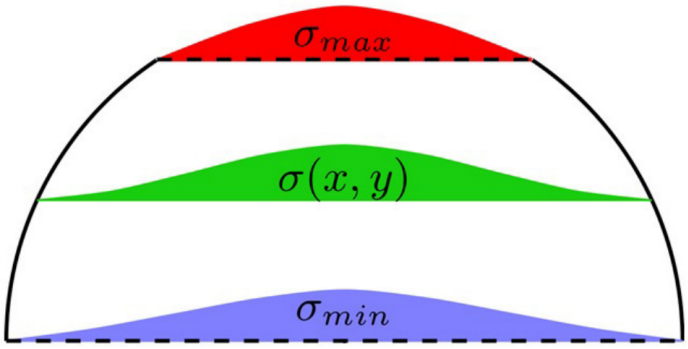

Figure 2.3: Stress profile of a cylinder acted on by a force point [29].

The sensing conductive plates could either be placed along the radius close to the edge, or along the curve. Both of these will be used in a design, by using two plates to sense the deformation for the first method, and by having small individual wires along the edge to try the second option. The two different designs can be seen in figure 2.4. The cylinders all have a diameter of 12.5 mm and a length of 10 cm, the plates have a thickness of 0.4 mm and the wires have a diameter of 0.8 mm. The small square bond pads are 5 mm × 5 mm with a thickness of 1.5 mm. The round bond pad has the same thickness, and a diameter of 10.5 mm. The loose sensor has the same dimensions as one of the plates in figure 2.4a.

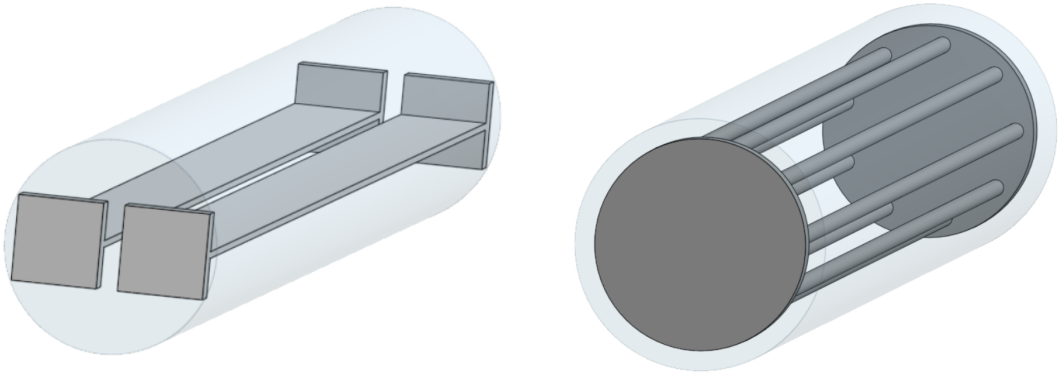

(a) Cylinder with 2 conductive plates and 4 bond pads. **(b)** Cylinder with conductive wires and 2 big bond pads.

Figure 2.4: The different sensor designs in cylinders.

2.6 Visualization

The greatest deformation was also visualized using a 3D printed TPU cylinder with differently coloured rings. It can be seen at rest and compressed in figure 2.5. The white rings are made of NinjaFlex [30], and the black rings are made of PI-ETPU [18], both have a similar tensile modulus so that the cylinder can be seen as a solid cylinder. As can be seen in the figure the greatest deformation in the black rings is towards the top and bottom of the cylinder. The rings closer to the center show little deformation. In accordance to the developed model by Asghar Aryanfar et al. [29] the center line has a greater deformation than its horizontal counterparts, supporting the decision on the placement of the sensors.

(a) Uncompressed cylinder made of NinjaFlex and PI-ETPU rings.

(b) Compression of a NinjaFlex cylinder with PI-ETPU rings to visualize the deformation.

Figure 2.5: TPU cylinders with rings to visualize deformation.

2.7 Fabrication

The sensors are fabricated with the designs displayed in figure 2.4, both laying down as displayed. One was fabricated with the design of figure 2.4a using using PI-ETPU as the conductive material. This design will be referred to as the plate sensor for the remainder of this work. The design in figure 2.4b was printed once with PI-ETPU as the sensor material as well and will be referred to as the wire sensor. The outside material the rest of the cylinder is made of is X60 [17] TPU for both of them. One of the conductive plates was also printed separately in PI-ETPU to do measurements on just the loose sensor itself. Figure 2.6a is the sensor with two plates firmly connected to the rest of the circuit using silver epoxy. The other side is connected

in the same manner. The cylinder with multiple wires can be seen in figure 2.6b, where wires can easily be connected using the screw and washer. Again, both sides were processed in the same manner. All designs were printed using the available Diabase H-Series. This printer is capable of printing with five different materials simultaneously, and uses a rotating turret with multiple nozzles to switch between materials. The slicer, a program that generates the GCode a 3D printer needs to print the 3D object, that was used is Ultimaker Cura 5.1.0 [31], and the settings for the two different materials can be found in table A.1 in Appendix A. Each print took about 6 hours to complete.

2.7.1 Quality

Due to the filament retaining some of its viscosity for a few minutes after extrusion, the nozzle from the Diabase passing over it can potentially drag some of it along. This created some unwanted connections between the bond pads of the plate sensor, and possibly the plates within. Connections on the inside would be impossible to remove without risking damaging the plates, but connections between the bond pads could be accessed from the outside and be removed. In addition to these extra connections, the individual traxels were still clearly visible, creating a lot of traxel to traxel connections, increasing the resistance. On the bond pads this resulted in a rough surface which would have a different resistance depending on the measured location. Hence this part would also require some more processing to equalize the potential. An example of visible traxels can be seen on the PI-ETPU strip in figure 2.7. The traxels formed by the different layers were still clearly visible on the individual bond pads, which can cause inconsistencies in the measurements.

2.7.2 Post-processing

The undesirable interconnections of the bond pads were carefully removed using a knife and tweezers. A resistance measurement with a multimeter, between the two plates, was used to validate that there is no short. A different solution, or prevention of this problem, would be to reprint the cylinders with the nozzle taking a different route during printing to reduce the stringing, which could also be accomplished by optimizing the print parameters, e.g. pressure and retraction. Another option is to print them in a different orientation to better separate the bond pads or reduce the size of the bond pads. This would also reduce the resistance of the sensors by having less traxel-to-traxel connections.

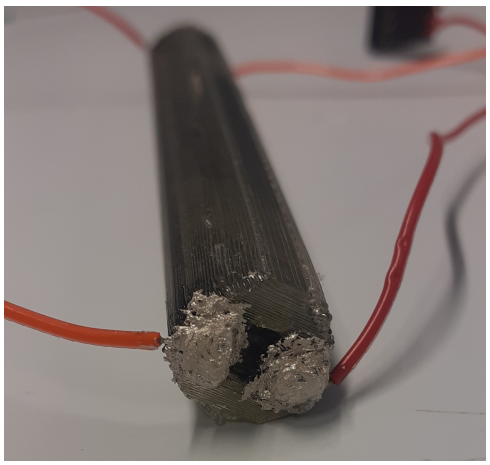

(a) Cylinder with 2 conductive plates and 4 bond pads connected with wires.

(b) Cylinder with conductive wires and 2 big bond pads with screws for connection.

Figure 2.6: The printed and processed designs.

To equalize the potential on the bond pads, silver ink [32] was manually deposited on top. Connecting the wires also proved to be a challenge, further supporting the additional investigation needed in the area of interfacing between 3D printed sensors and traditional electronics [13]. The cylinder with the wires had a small hole drilled in the middle, where it would not touch any of the internal connections. The wires could then be connected with a small screw and a ring washer as to secure the connection wires. This did increase the resistance to 135 kΩ. The resistances of the other sensors are displayed in table 3.1. The loose sensor simply had the wires soldered/melted to the material. The bond was strong enough for measurements, but not for long lasting applications. The bond pads on the plate sensors were too small to take the same approach of drilling a hole. The connections to the two plates in the cylinder were similar to how the strip sensor was connected, but included applying silver epoxy [33] to secure the bond. The processed and connected sensors can be found in figures 2.6 and 2.7.

Figure 2.7: The soldered loose plate sensor

2.8 Conclusion

In the end it was decided to use two different designs following from stress profiles produced by the discussed model in two cylinder shapes. A torus shape would be a closer resemblance to the real situation, but becomes too complicated for the scope of this work. To mimic some of the known forces, the cylinders will be compressed on the cross-section during measurements.

3 Measurements

3.1 Introduction

In this chapter, the experimental setup used to characterize the sensor is described. All relevant parameters are introduced, and the results are discussed. From these results, the resistance and relative resistance change is calculated.

3.2 Measurement setup

To test the sensors in the cylinders, the resistance will be monitored while an actuator exerts pressure on the cross-section. The resistance change is measured using a half-bridge circuit. The main pieces of equipment used are listed below.

- Linear actuator (SMAC LCA25-050-15F) [34]
- Load-cell (LCMFD-50N) [35]
- Data Acquisition System (DEWE-43A V21-2)
- Programming platform (MATLAB 2021a)
- Voltage Output Load Cell Amplifier (IAA100) [36]

To realize the interfaces between the main equipment, the following components are employed:

- 2× RS232 9-pin connectors
- 4× resistors (33 kΩ, 130 kΩ, 330 kΩ and 390 kΩ)
- Silver ink
- Silver epoxy

The SMAC linear actuator is used to control the exerted force on the cylinder, and the load-cell in between the SMAC and the cylinder measures this applied force more accurately. The DEWE-43 measures these two signals (the force from the load-cell as well as the SMAC translation), along with the measured voltage from the sensor half-bridge circuit to easily synchronize the signals. In the case of the cylinder with two plates there were two similar half-bridge circuits for both sides. The realized circuit is adapted from the DEWE manual [37] for a 3-wire-sensor connection and an excitation voltage of 10 V, see figure 3.1. The sensor field on the right in this figure contains the bridge resistor R_{br}, which is different for each sensor part. R_{s} indicates the measured resistance of the fabricated sensor, either the plate or the combined wires. This circuit was used twice for the sensor with plates, one for each. The connector field on the left indicates the RS232 9-pin connector. One side went into the analog connections of the DEWE, the other was connected to the circuit as indicated.

The resistances of the sensors at rest (R_0) and the used bridge resistor (R_{br}) can be viewed in table 3.1. The resistances were measured about two to three weeks after fabrication, so that they had time to settle into a relatively consistent resistance. This is important since other experiments from the NIFTy group revealed that there is a significant drop in resistance after the fabrication. Another option to stabilize the resistances would be to anneal the sensors in an oven. Ideally the bridge resistors are as close as possible to the resistance of the sensor at rest to improve the balancing. This is not the case for the plate resistors however. The bridge resistors were decided before the sensors were fully prepared and attached to the circuit, modifying

the resistance. In retrospect this should have been taking into account before choosing the bridge resistors. To improve the results when continuing this research, this should be done more carefully.

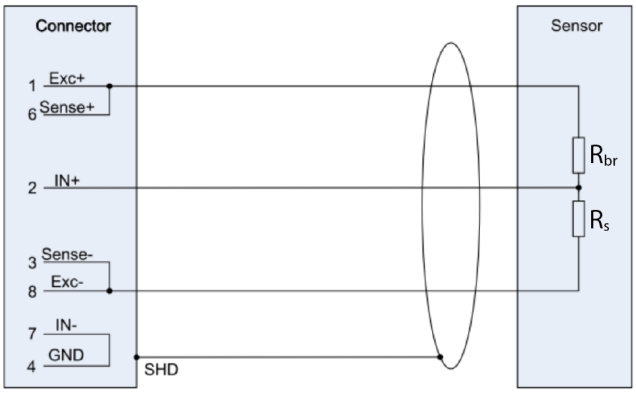

Figure 3.1: Half-bridge circuit for a 3-wire-sensor connection with an excitation voltage of 10 V adapted from the DEWE manual [37].

Sensor	R_0 (kΩ)	R_{br}(kΩ)
Wire sensor	135	130
PI-ETPU strip	30	33
Plate sensor		
top	220	330
bottom	280	390

Table 3.1: Values for R_{br} and R_0.

The last pieces necessary for experimentation were the support pieces; a concave tip attached at the actuator's stroke endpoint, and a basis mount bracket for the sensors to rest upon. These designs can be seen in figure 3.2. Figure 3.2a shows the base the cylinders will rest on, with a long concave slit matching the curvature of the cylinders so that a long slice with an angle of 45° is resting in the slit in the base, the same angle as the actuator piece in figure 3.2b uses. For the PI-ETPU strip sensor, the base was flipped as to provide a flat rigid base, and the actuator tip used is seen figure 3.2c (c). The entire setup is assembled on an aluminum plate with threaded bores located in a grid on the surface for easy assembly. The full setup for the wire sensor and the loose PI-ETPU strip sensor can be seen in figure 3.3. The box indicating the SMAC is currently focused on the stroke of the actuator.

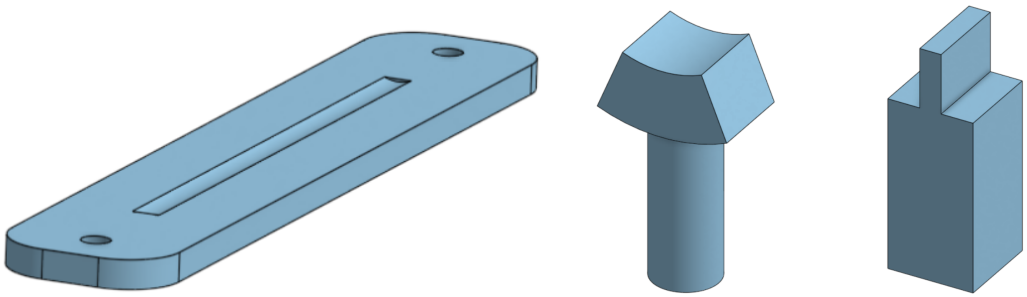

(a) Support piece for the cylinders.

(b) Support for on the actuator for cylinders.

(c) Support for on the actuator for a flat sensor.

Figure 3.2: Support parts.

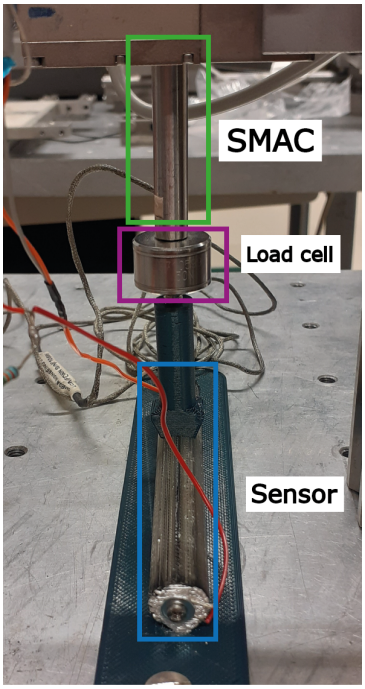

(a) Setup for the wire sensor.

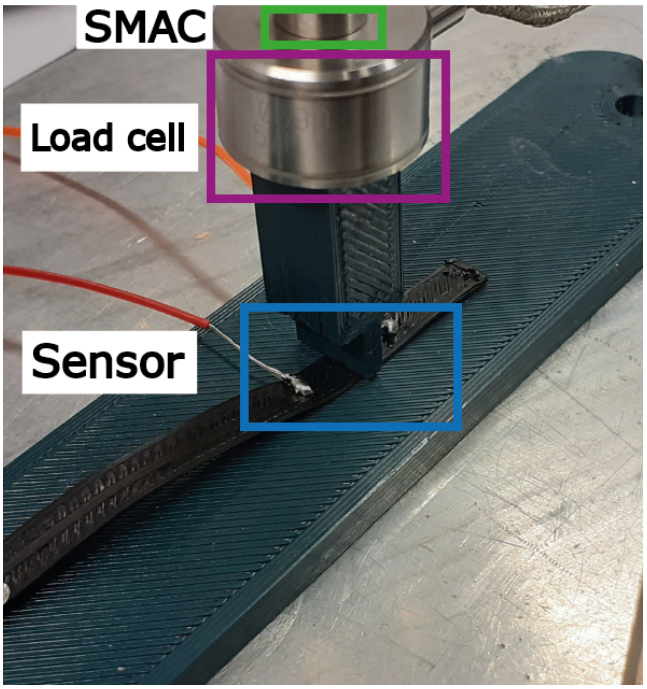

(b) Setup for the loose sensor.

Figure 3.3: Setups for the wire and loose sensor. In the green box the SMAC actuator, the load cell in purple and the part of the sensor that is measured in blue.

The plate sensor was also placed into the slit in the supportive base at first, similar to the wire sensor. Five different orientations were identified compared to the actuator, see figure 3.4. The first configuration, 0°, has both plates reside in the x-z plane (figure 3.4a). In the second configuration, 45°, the plates have a 45° angle with the x-axis as in figure 3.4b. When the plates are vertical compared to the x-z plane (figure 3.4c), the plates are at a 90° angle. Rotating the other direction with the z-axis as the rotational axis will be considered the negative versions of these angles, with the blue sensor being the top one.

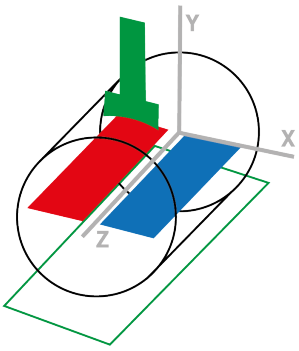

(a) Setup plate sensor in horizontal orientation.

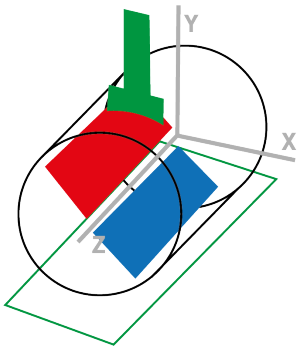

(b) Setup plate sensor in 45° orientation.

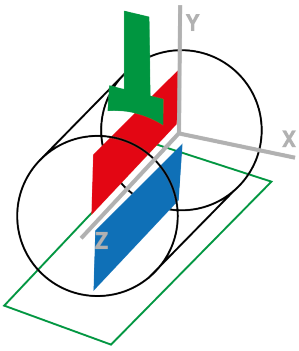

(c) Setup plate sensor in 90° orientation.

Figure 3.4: Schematics of the experimental setup for the plate sensor. The two sensors in red and blue, and the actuator and base in green.

Although the wire sensor would theoretically be perfectly symmetrical, inaccuracies during printing and the generated slicing pattern possibly lacking this symmetry ensure the reality will deviate. Every wire in the cylinder will be slightly different, and produce a different response. This difference was not investigated in this work, but could be an interesting topic for further research. Half of the generated slicing pattern can be seen in figure 3.5. Simply looking at the

top of the grey wires reveals differently generated traxels for theoretically the same shape due to the filament having a thickness of 0.2 mm.

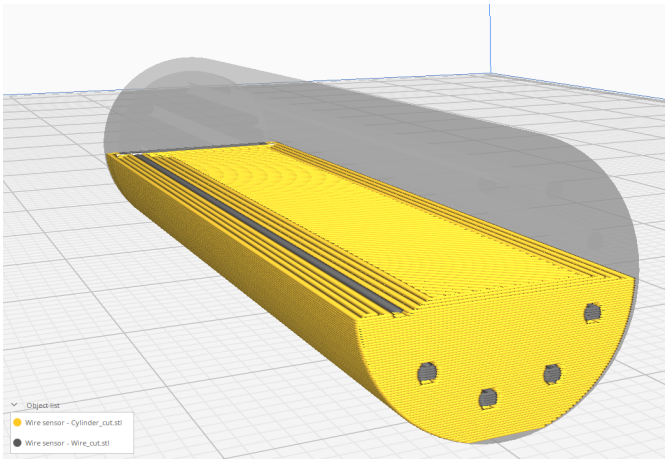

Figure 3.5: Half of the slicing pattern generated by UltiMaker Cura of the wire sensor. In yellow the X60 TPU and the PI-ETPU in grey.

3.3 Measurement procedure

Once all connections were made and all components were in place, the measurements were controlled by MATLAB and DEWESoft. The MATLAB scripts that were used can be found in appendix C. The actuator allows the use of either position control or force control. In this case force control was used, with an amplitude of 4 N and an offset of 6 N as sinusoidal input signal to ensure the actuator would not lose contact with the sensor during measurements. Other relevant parameters can be found in table 3.2. For the first measurements on the loose PI-ETPU strip sensor and the wire sensor, the external amplifier (IAA100) was used with an 10 V excitation voltage. The measurements on the plate sensors use a build-in amplifier from the DEWE for half-bridge measurements, with a Butterworth low-pass filter of the 2nd order of 1 kHz and a bridge resistance of 350 Ω.

Parameter	Value
Sample rate	20 000 Hz
Amplitude input	4 N
Offset	6 N
Frequency	0.1–0.5 Hz

Table 3.2: Relevant parameters during measurements.

3.4 Adaptations

During measurements it became evident that the printed support plate did not provide the necessary constrain and the cylinder could move and visibly deflect under pressure. In addition, the 3D printed base could not be screwed to the grounded plate completely flush due to measurement and fabrication errors (warping), which introduced additional unwanted movements. To combat some of these issues, the support piece was removed, and the flat aluminum clamping plate became the new base. Kapton tape was used to offset and isolate the sensor from the ground plate. Two pieces of cardboard were screwed over the cylinder to keep it from moving. They were not screwed on too tight to prevent initial compression, but they did prevent turning of the cylinder during measurements. Reprinting the support pieces would have been a more elegant solution, but time did not allow for this. For the same reason, this new

setup, as can been seen in figure 3.6, was only used for the plate sensor, and for measurements with an excitation frequency of 0.5 Hz.

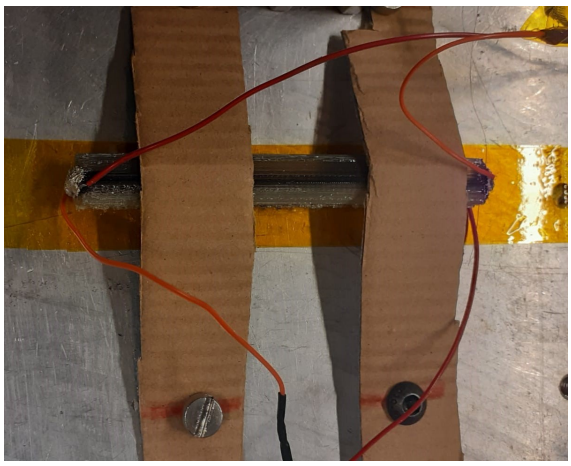

Figure 3.6: New setup for the plate sensor.

3.5 Results

Only the measurements using an input signal of 0.5 Hz will be used in the calculations since the observed behaviour is not significantly different at lower frequencies, and because the latest measurements on the plate sensor only used this frequency. The responses from the other measured frequencies can still be found in appendix B. Figure 3.7 shows the responses and input for the wire sensor and the loose strip. Only the middle part of the measurements is shown. All responses exhibit the same peculiar behaviour, showing an extra bump every oscillation. This very same behaviour can also be found in the response of the loose PI-ETPU strip sensor, see figure 3.7b. Only this time the peak is more prominent.

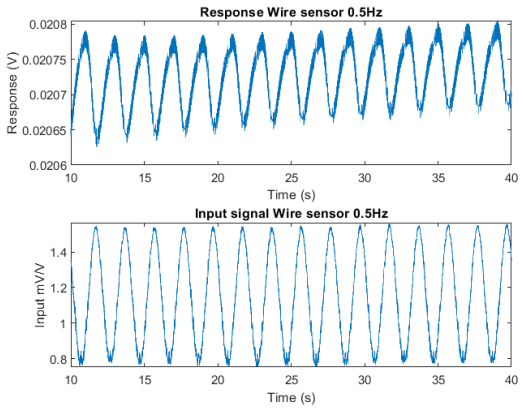

(a) Response and input for the wire sensor at 0.5 Hz.

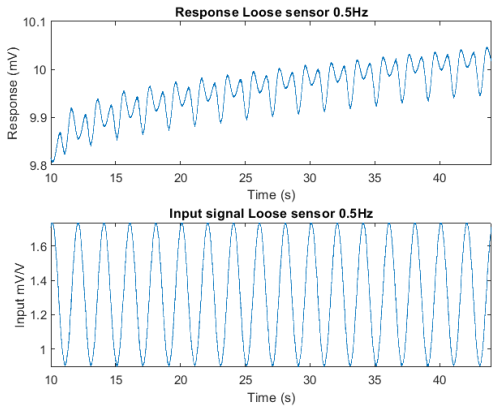

(b) Response and input for the loose sensor at 0.5 Hz.

Figure 3.7: Response and input for the 2 simpler sensors

The first measurements on the plate sensor with the first setup using the support pieces can be seen in figure 3.8. The new measurements are plotted in more detail in figures 3.9 and 3.10. In these plots it becomes evident that the general shape of the graphs was not heavily influenced by the less constrained setup. Hence the results from the wire and loose sensor can still be used to provide insight in the responses from the designs. For further calculations on the resistances the newer results will be used.

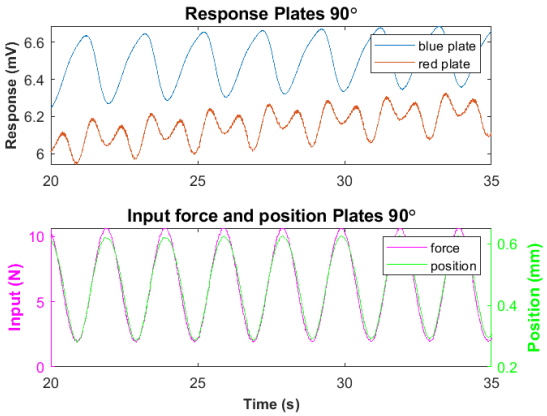

(a) Response and input for the plate sensor at 0.5 Hz at 90°.

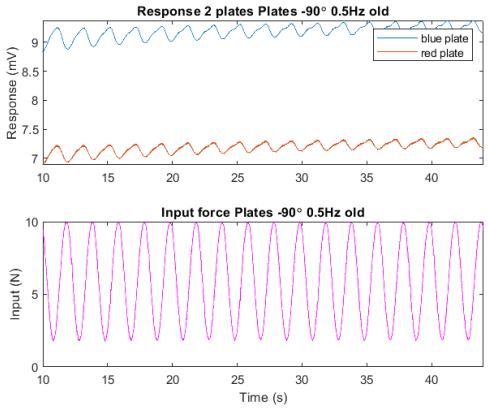

(b) Response and input for the plate sensor at 0.5 Hz at −90°. The position was not working correctly.

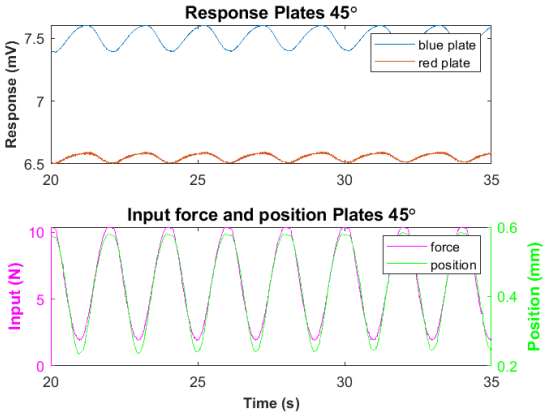

(c) Response and input for the plate sensor at 0.5 Hz at 45°.

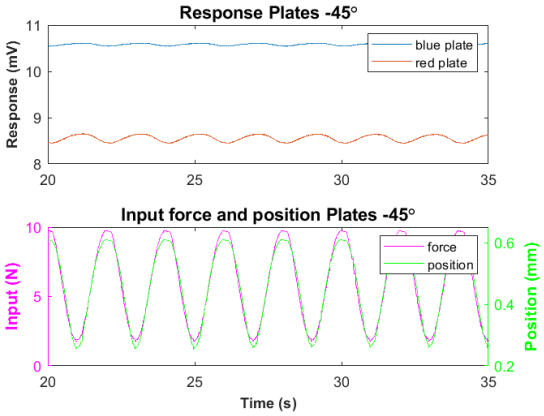

(d) Response and input for the plate sensor at 0.5 Hz at −45°.

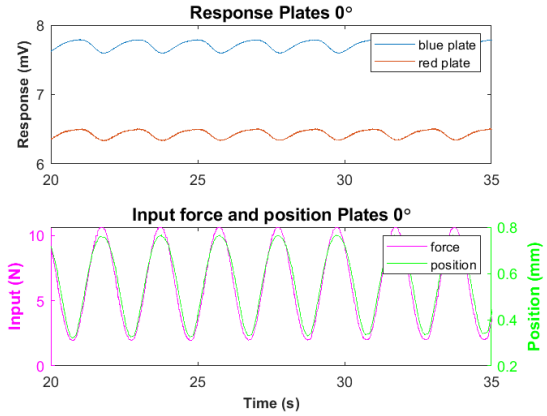

(e) Response and input for the plate sensor at 0.5 Hz at 0°.

Figure 3.8: Original response and input for the plate sensor at various angles.

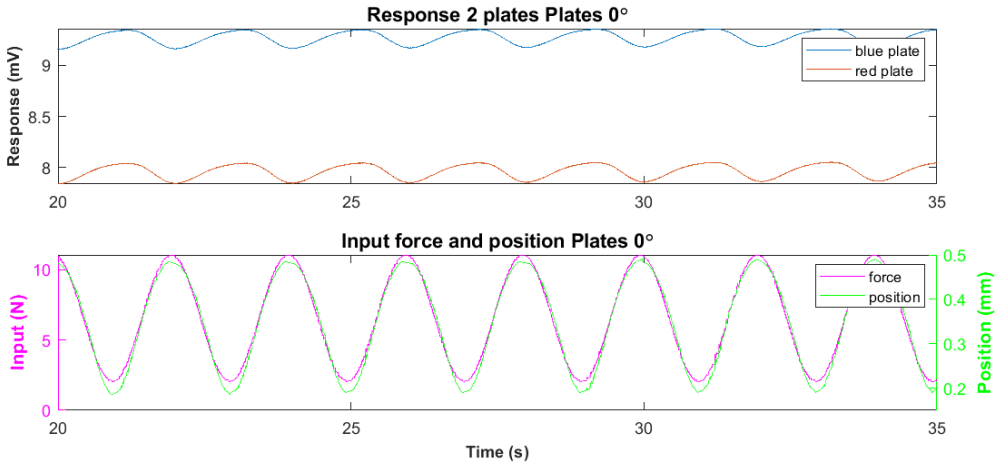

(a) Response and input horizontal plates.

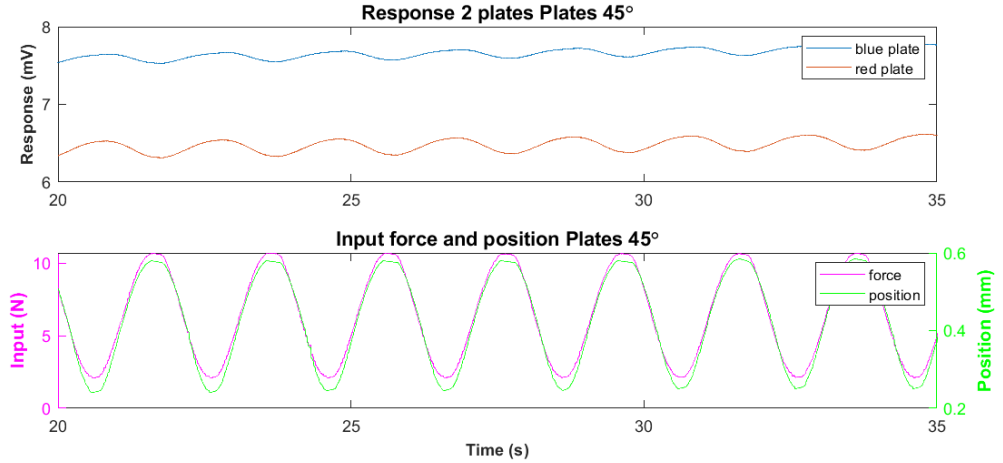

(b) Response and input plates at 45°.

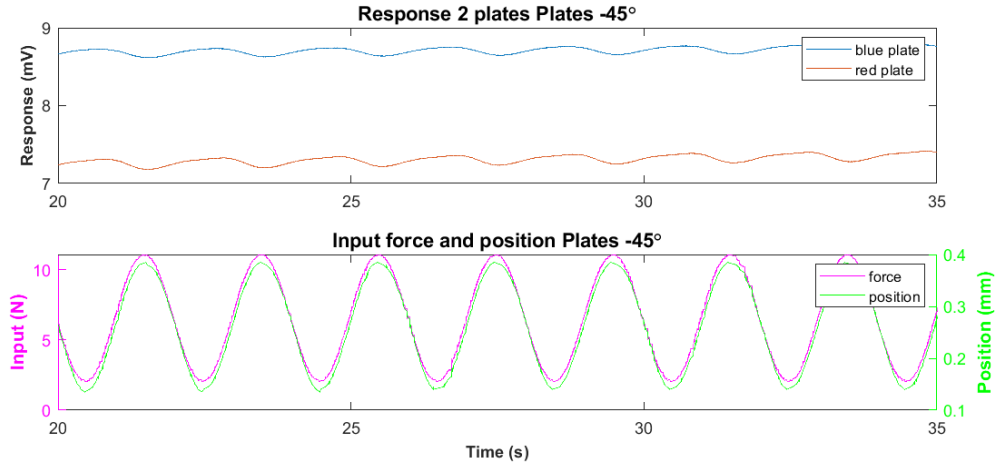

(c) Response and input plates at −45°.

Figure 3.9: Response and input for plate sensor horizontally and at ±45°

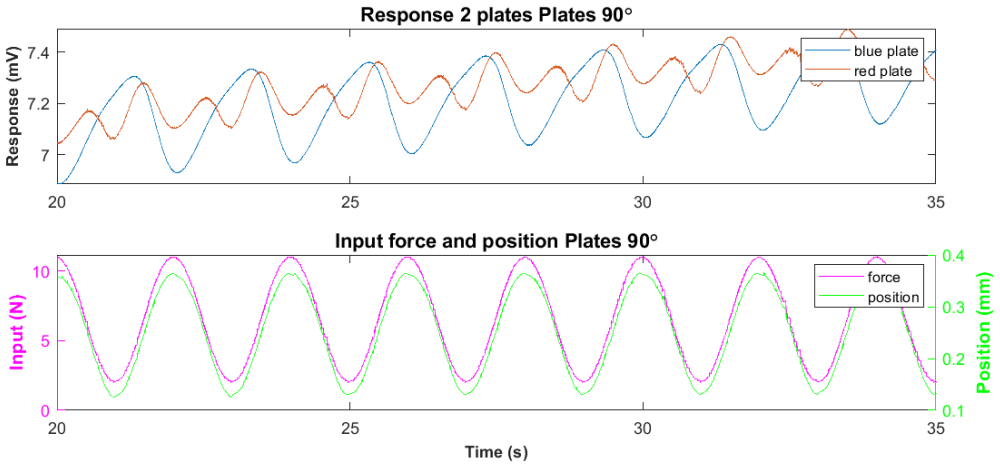

(a) Response and input plates at 90°.

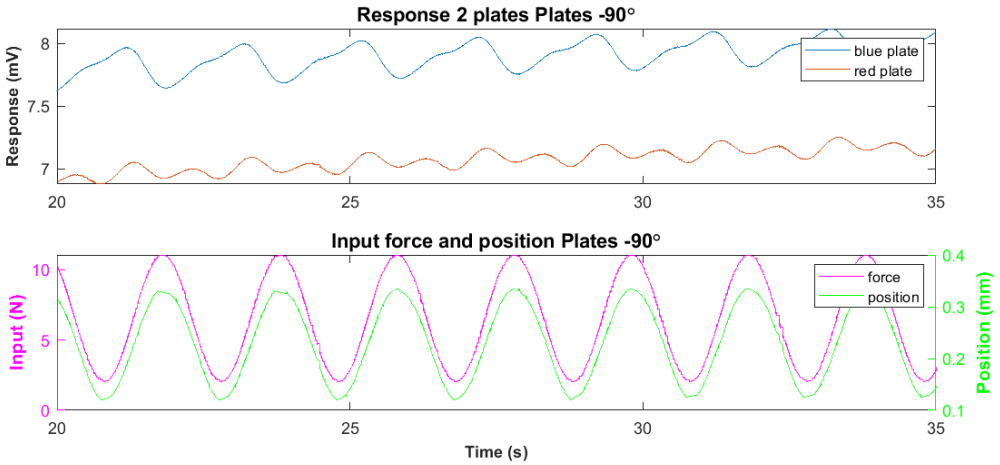

(b) Response and input plates at −90°.

Figure 3.10: Response and input for plate sensor at ±90°

All fabricated sensors seem to exhibit the similar behaviour where there is an extra peak every oscillation. Interestingly enough it turns out that this is slightly more evident when the conductive plate in the plate sensor is closer to the top, or closer to the actuator. Looking at the results from the loose sensor, which is as close to the actuator as can be, supports this conclusion. Part of it does come from the specific properties of the structure as the difference between the top and bottom plate is not as obvious in figure 3.10b as it is in figure 3.10a. Since the cylinders were not perfectly constrained in every direction during the measurements, it is possible that the entire cylinder started bending slightly, causing this peculiar behaviour of the additional peaks. To analyze this specific source of deformation, additional experiments are required. Ones that elevate the cylinder to bend it and focus on this deformation for example. This shape is not entirely new however, as others have observed a similar shape [38]. The exact reason for this behaviour is still unknown, but a possible explanation could be that the ends of the cylinders do actually oscillate as well, just too small for the naked eye to see.

3.5.1 Resistance and relative resistance change

From the voltage obtained from the measurements, the resistance of the sensor in the half-bridge configuration (see figure 3.11) can be obtained by the following formula, where V_m represents the measured voltage, R_{br} the bridge resistor, R_s the resistance of the sensor, and V_0

is half of the excitation voltage of 10 V. If Exc+ and Exc- had different magnitudes they would need to be considered separately.

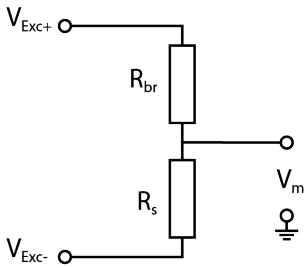

Figure 3.11: Half-bridge configuration with single sensor.

$$V_{\mathrm{m}} = \frac{R_{\mathrm{s}} - R_{\mathrm{br}}}{R_{\mathrm{s}} + R_{\mathrm{br}}} V_0 \tag{3.1}$$

To get the resistance of the sensor, the equation can be rewritten as below.

$$R_{\mathrm{s}} = -R_{\mathrm{br}} \frac{V_{\mathrm{m}}/V_0 + 1}{V_{\mathrm{m}}/V_0 - 1} \tag{3.2}$$

The relative resistance change $\Delta R/R$ can be calculated using the following equation.

$$\frac{\Delta R}{R} = \frac{R_{\mathrm{s}} - \hat{R}_{\mathrm{s}}}{\hat{R}_{\mathrm{s}}} \tag{3.3}$$

With $\hat{R}_{\mathrm{s}}$ being the mean of the resistances with n the number of data points, given by:

$$\hat{R}_{\mathrm{s}} = \frac{1}{n} \sum_{k=1}^{n} \hat{R}_{\mathrm{s}_k} \tag{3.4}$$

Applying these equations to the obtained results and values of the bridge sensors (table 3.1) results in the resistance (R) and relative resistance change ($\Delta R/R$) of the wire sensor in figures 3.12a and 3.12b respectively. The results from the loose sensor in figures 3.13a and 3.13b exhibit the same behavior.

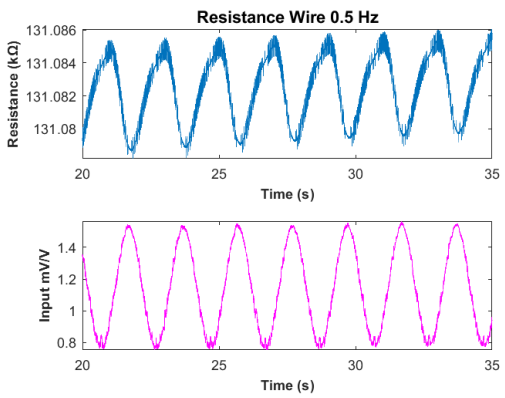

(a) Resistance of the wire sensor at 0.5 Hz and input.

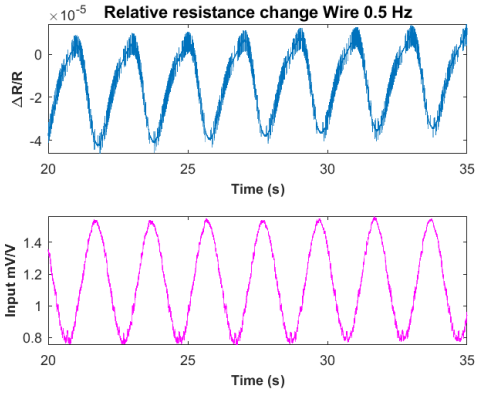

(b) Relative resistance change of the wire sensor at 0.5 Hz and input.

Figure 3.12: Resistance and relative resistance change of the wire sensor and input.

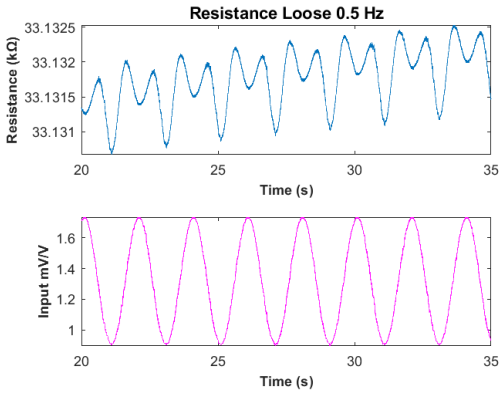

(a) Resistance of the loose sensor at 0.5 Hz and input.

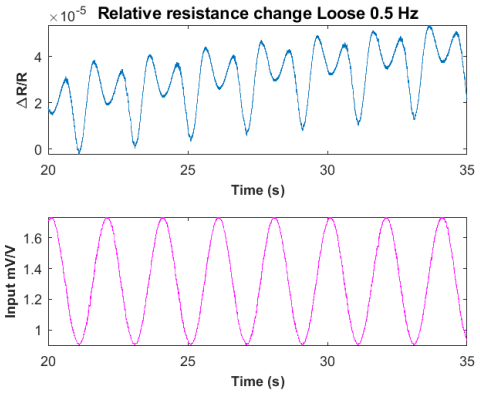

(b) Relative resistance change of the loose sensor at 0.5 Hz and input.

Figure 3.13: Resistance and relative resistance change of the loose sensor and input.

Figure 3.14 shows the relative resistance changes for the angles 0° and 90° for both plates in the plate sensor. As is to be expected, these also show the same behaviour. The absolute resistances are not as much of interest, so they have been place in appendix B in figure B.3.

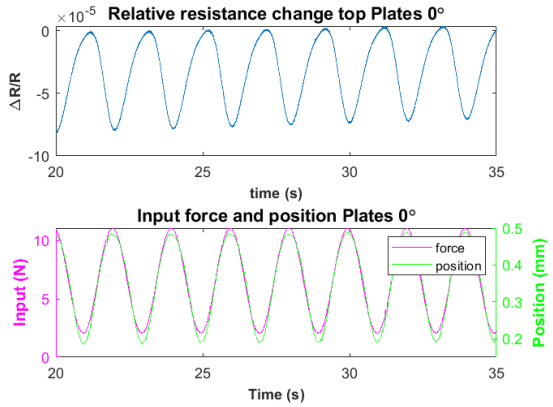

(a) Relative resistance change 0° for the top plate with input.

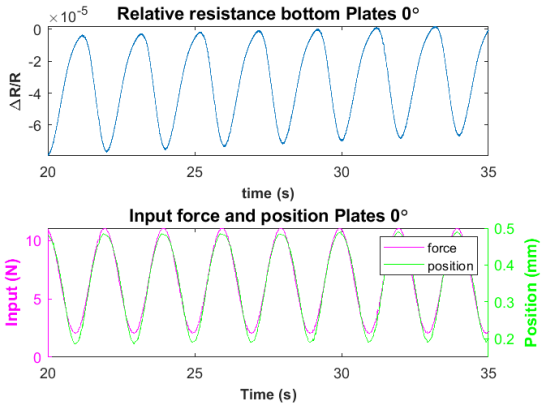

(b) Relative resistance change 0° for the bottom plate with input.

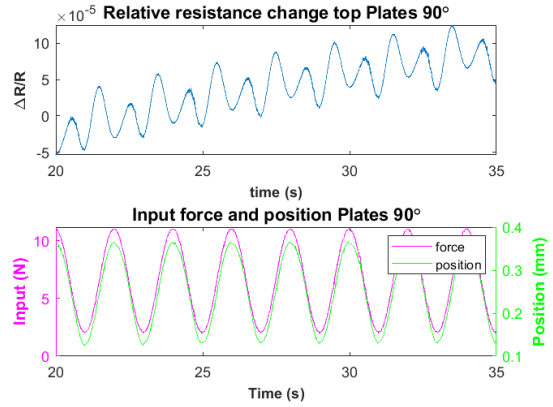

(c) Relative resistance change 90° for the top plate with input.

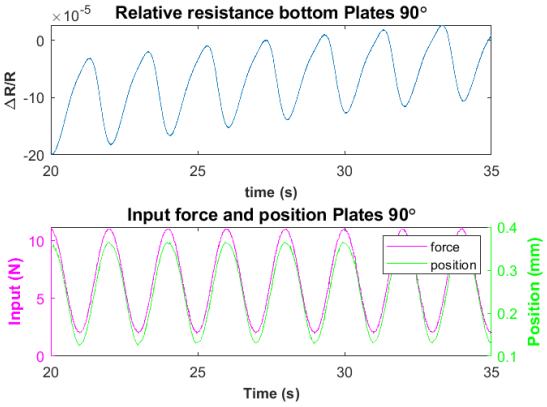

(d) Relative resistance change 90° for the bottom plate with input.

Figure 3.14: Some relative resistance changes for 0° and 90° with input.

3.5.2 Hysteresis

Whether a system is dependent on it's past can investigated using hysteresis plots. Hence these were also made regarding the sensors. Since the position was not working correctly for the wire sensor and strip, $\Delta R/R$ was plotted against the force. See figure 3.15. Both sensors show dependence on their past.

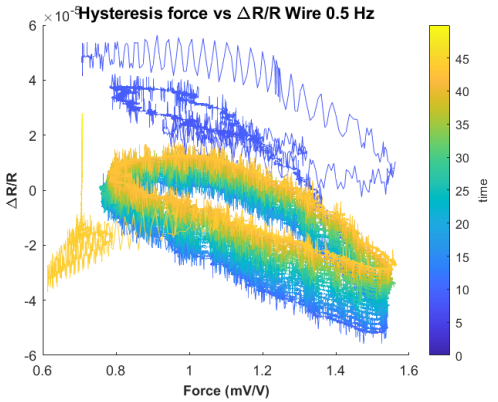

(a) Hysteresis wire sensor.

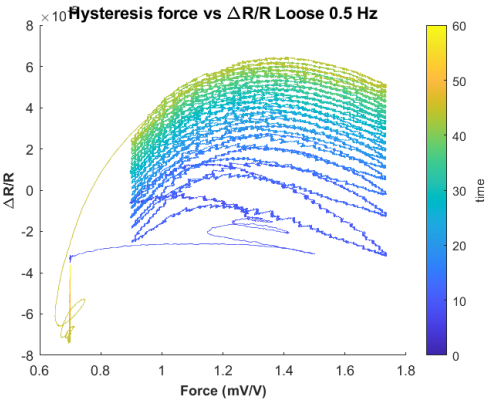

(b) Hysteresis loose sensor.

Figure 3.15: Hysteresis plots wire and loose sensor of relative resistance change versus input force.

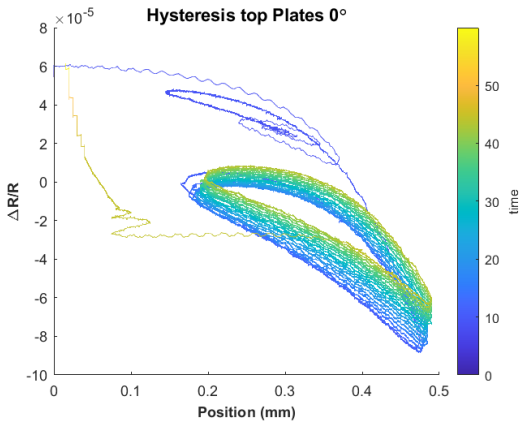

(a) Position vs relative resistance change for the top plate at 0°.

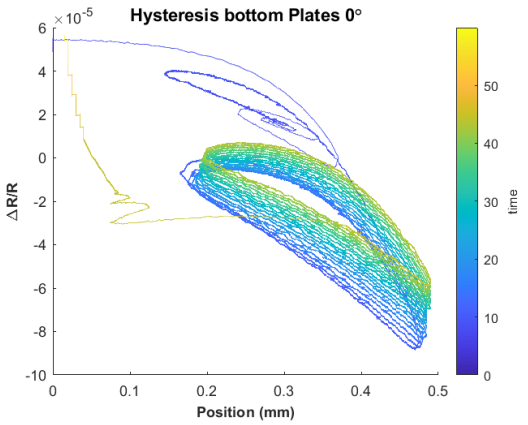

(b) Position vs relative resistance change for the bottom plate at 0°.

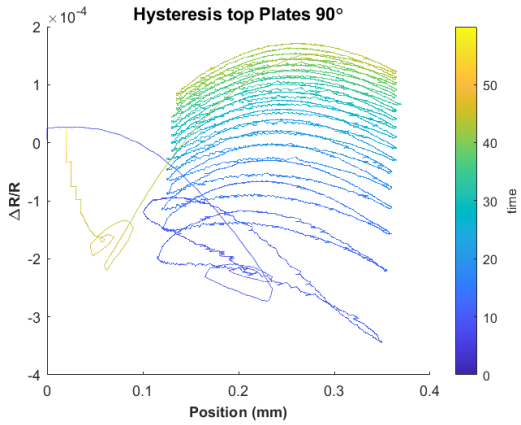

(c) Position vs relative resistance change for the top plate at 90°.

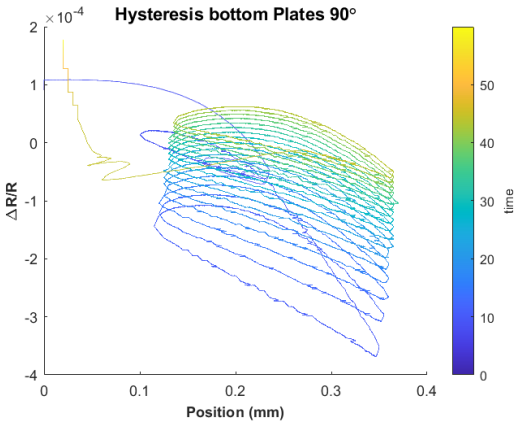

(d) Position vs relative resistance change for the bottom plate at 90°.

Figure 3.16: Hysteresis plots of the plate sensors at 0° and 90° of position vs $\Delta R/R$.

Plots against the position can bee seen in figure 3.16 for the horizontal and vertical orientation of the plates. The later exhibits hysteresis more obviously.

3.6 Conclusion

The performed experiments and the results are described and presented. Due to the originally used support pieces not providing the necessary constraints, a new setup was made. This setup was only used for the plate sensor, and when comparing the new results to the old ones, the overall shape of the graphs was still the same. The non-optimal setup did not invalidate the previously acquired results. The results do seem to have drift, this could possibly have been alleviated by using a differential measurement. The relative resistance changes indicate that it is possible to sense a deformation, and that this could be an interesting approach for further research to develop.

4 Conclusions and recommendations

The goal of this research was to attempt to design and fabricate a structure (torus) capable of sensing mechanical deformations. More comprehensive models describing the forces on a torus shape quickly became too complicated for the scope of this work. So to simplify the situation for both modelling and testing the torus shape was changed to a cylinder. In these cylinders the sensors were embedded to then be subjected to compression as if the cylinder were pinched. Out of a piezoresistive and capacitive configuration the first option was chosen because of the simpler implementation. The location of the conductive materials was determined using the work of Asghar Aryanfar et al. [29] to determine the location of the greatest stress. The results seem to indicate that the two tested designs could indeed determine when the structure was being deformed. The resulting shapes of the graphs do hint at the other phenomena being at work however. More research is required to pinpoint the source of this and to learn more about how it will influence the sensors and if it could be used as an advantage.

Some improvements could have been made during this research if time allowed it. The setup had some undesired effects that could have influenced the results. In addition some extra experiments on the fabricated sensors would have provided more insight on the underlying phenomena. Producing some plots around the concept of hysteresis is another important aspect that was omitted in this work due to time, but could have improved the understanding of the quality of the sensors. A final point that would improve the results is to use a differential measurement to remedy the drift.

The eventual goal of getting a better grasp on the workings of pessaries by using electrical sensors will still require more developments and improvements in the field. Possible topics for further research could be the location of the sensor, the type of sensor or how to further optimize the printing process.

A Settings

Material	X60	PI-ETPU
Extrusion temperature (°C)	215	225
Build plate temperature (°C)	60	60
Layer height (mm)	0.2	0.2
Initial Layer height (mm)	0.3	0.3
Line Width (mm)	0.45	0.48
Initial Layer Speed (mm/s)	7.5	7.5
Print Speed (mm/s)	15	15
Flow (%)	125	100
Infill Density (%)	100	100
Infill Pattern	Lines	Lines

Table A.1: Settings of the Diabase for the two materials

B Experimental results

B.1 Wire sensor response

Figure B.1 shows the input and response of the wire sensor for the frequencies between 0.1–0.4 Hz.

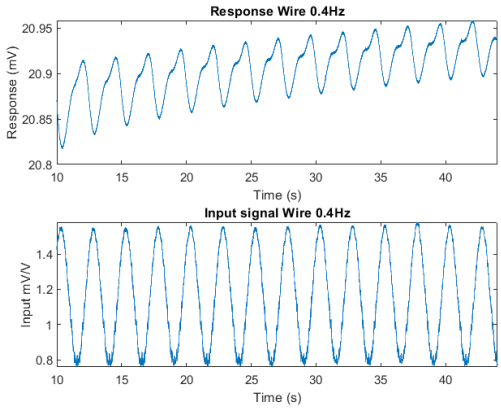

(a) Response and input for the wire sensor at 0.4 Hz.

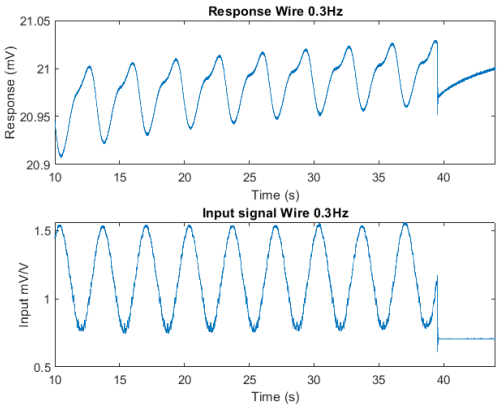

(b) Response and input for the wire sensor at 0.3 Hz.

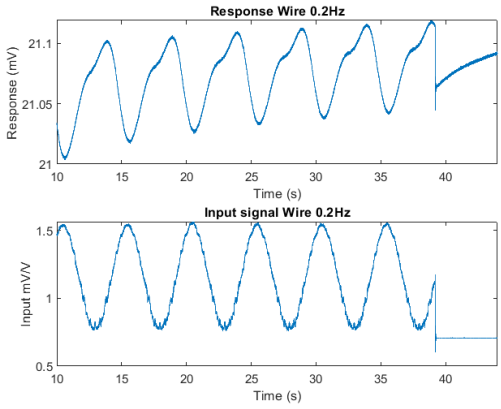

(c) Response and input for the wire sensor at 0.2 Hz.

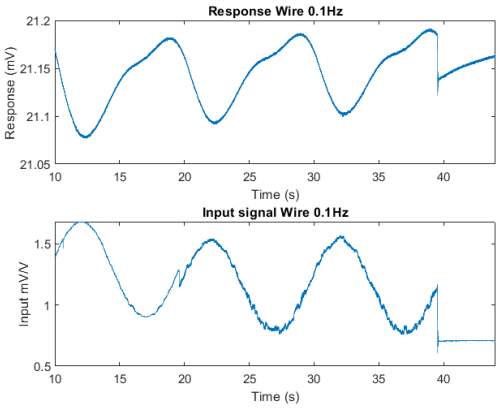

(d) Response and input for the wire sensor at 0.1 Hz.

Figure B.1: Response and input for the wire sensor between 0.5 and 0.1 Hz

B.2 Loose sensor response

Figure B.2 shows the input and response of the strip sensor for the frequencies between 0.1–0.4 Hz.

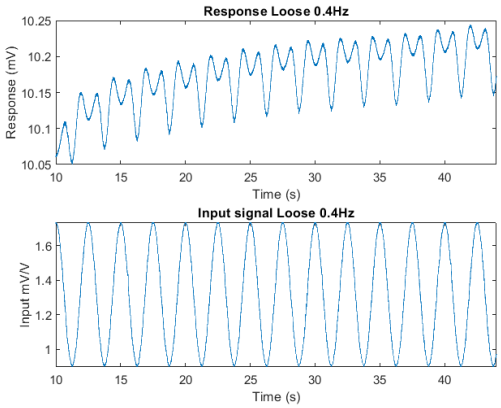

(a) Response and input for the loose sensor at 0.4 Hz.

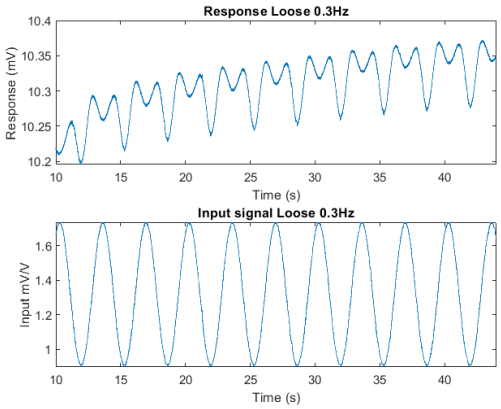

(b) Response and input for the loose sensor at 0.3 Hz.

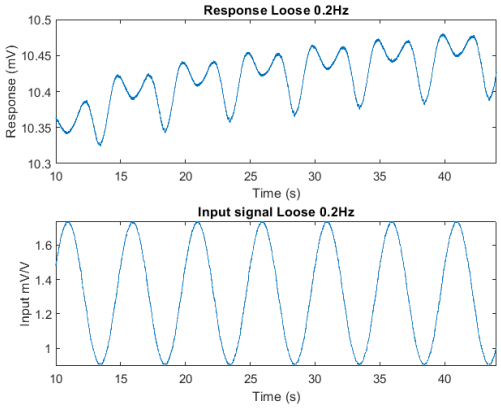

(c) Response and input for the loose sensor at 0.2 Hz.

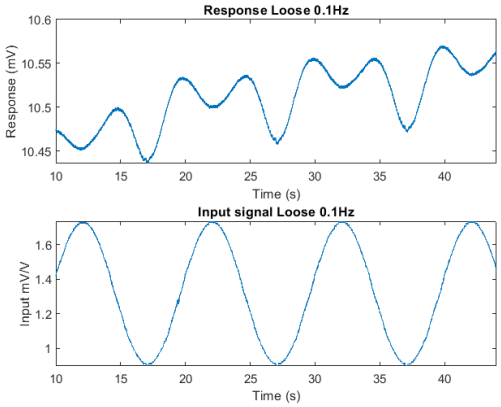

(d) Response and input for the loose sensor at 0.1 Hz.

Figure B.2: Response and input for the loose sensor between 0.5 and 0.1 Hz

B.3 Resistances of plate sensor

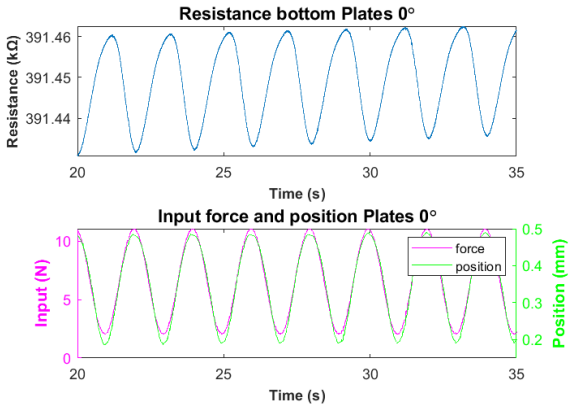

(a) Resistance 0° for the top plate with input.

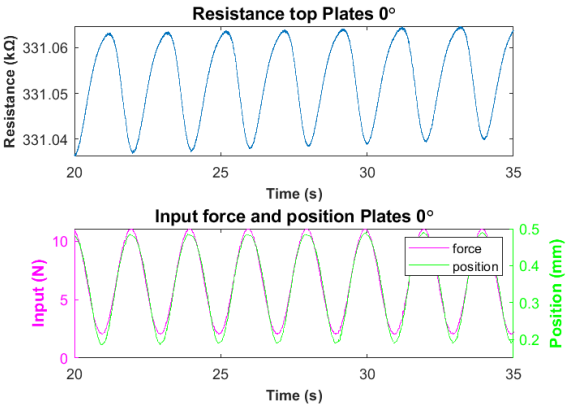

(b) Resistance 0° for the bottom plate with input.

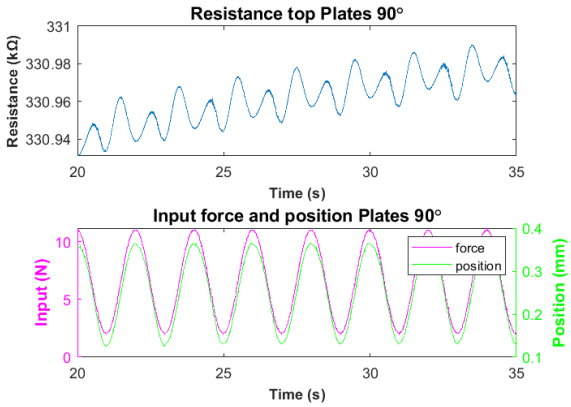

(c) Resistance 90° for the top plate with input.

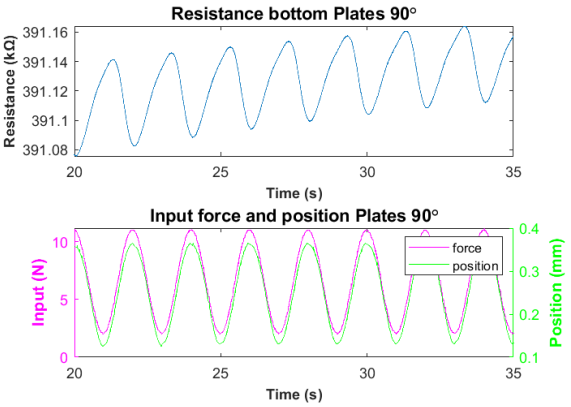

(d) Resistance 90° for the bottom plate with input.

Figure B.3: Some resistances of the plate sensors for 0° and 90° with input.

C MatLab scripts

C.1 Main script for reading the DEWE

```
%% Reading & Storing of measurement data from DEWE-43A
%
% Reads and stores data from DEWE-43A to .mat & .d7d files
%
% Equipment: [1] DEWE-43A : User defined amount of analog
   channels
%
% Author: Dimitris Kosmas


% clear old variables
clearvars;
close all
load counter;

SR = 20000; % sample rate
start_calc = 0;

time = 50; % [s], experiment time

% global actx
% global ReadCh;

% DeweSoft server initialization
actx = actxserver('Dewesoft.App');
actx.Init();
actx.Visible = true;
actx.Width = 1200;
actx.Height = 600;

actx.SetupScreen;

pause; % pause for manual inputs
%%
% number of all channels
fprintf('\n');
display(['Number of all channels: ', num2str(actx.Data.
   AllChannels.Count)]);

% list of all channels
disp('List of all channels:');

actx.Data.AllChannels.Item(1)

% set the used channels to used
for i = 0 : actx.Data.AllChannels.Count - 1
```

```
    ChName = actx.Data.AllChannels.Item(i).Name;
        disp(ChName);

    % we are going to read data from AI 1 channel
    if (strcmp(ChName, 'AI 1'))
        ReadCh = actx.Data.AllChannels.Item(i);
        ReadCh.Used = true;
    end
    % second channel
    if (strcmp(ChName, 'AI 2'))
        ReadCh = actx.Data.AllChannels.Item(i);
        ReadCh.Used = true;
    end
    % only use this channel for the two plates
    if (strcmp(ChName, 'AI 3'))
        ReadCh = actx.Data.AllChannels.Item(i);
        ReadCh.Used = true;
    end
    % digital input for position from SMAC
    if (strcmp(ChName, 'CNT 1/Count'))
        ReadCh = actx.Data.AllChannels.Item(i);
        ReadCh.Used = true;
    end
end

%%

% Store data
path =  "C:\Users\NIFTy_PC1\Downloads\MeasurementsLarissa\
   data\raw\DEWE\";
filename = string(path+"\data_"+mat2str(counter)+".d7d" );
actx.StartStoring(filename);
pause(time);
actx.Stop();
actx.LoadFile(filename);

% Data readout
data_sections = actx.LoadEngine.DataSections;
disp(sprintf('Number of data sections %d', data_sections.
   Count));
data_section = data_sections.Item(0);

sample_rate = actx.Data.SampleRate;
disp(sprintf('Sample rate: %d', sample_rate));

% Read number of channels in Dewesoft
channel_count = actx.Data.UsedChannels.Count;
disp(sprintf('Number of channels: %d', channel_count));

% Go through all channels and extract data
for i = 0:channel_count - 1
```

```
        ch = actx.Data.UsedChannels.Item(i);

        % Get number of samples for channel
        sample_cnt = data_section.DataCount;

        % If there is some samples in the data file then read
           sample values and
        % Corresponding time stamps (also synchronous channels
            have timestamps)
        if sample_cnt > 0
            [out_data(:,i+1), out_time_stamp] = data_section.
               ReadData(ch);
            if isnan(out_time_stamp)
                t(:,i+1) = [0:1/sample_rate:(sample_cnt - 1)/
                   sample_rate];
                data(:,i+1) = out_data(:,i+1);
            end

        end
    end

    %Plot data from channels
    figure(1)
    for i1= 1:channel_count-1
        subplot(channel_count-1,1,i1)
        plot(t(:,i1),data(:,i1))
    end

    title(sprintf('Number of channels: %d', channel_count));

    % Deactivate channels in DEWE-43A
    for i = 0:20
        actx.Data.AllChannels.Item(i).Used = false;
    end

    % clear actxserver object
    actx = 0;

    % Save data : t, data
    % Only save one column of t
    t = t(:,1);
    save(['data\raw\DEWE\','data_',mat2str(counter),'.mat'], '
       t', 'data')

    % Increment counter
    counter = counter +1;
    save('counter.mat','counter');
```

C.2 Script for controlling the SMAC actuator

```
function smac_control(time)
```

```
% Check for open connections
try fclose(actuator); end

instrreset;

load counter_smac;

PperP = 0.0051; % Converstion SMAC to Position

% SMAC related initialization
   ========================================
SMACport = 7;

actuator = SMAC_init(SMACport); % Call SMAC_init
   function

% Find start position
fprintf(actuator, '32 R 0X006064');%read position
start_position = strsplit(fgets(actuator),' ');
start_position = str2double(start_position(end)); %
   start_position !

fprintf(actuator, '32 R 0X006077');%read force
start_force = strsplit(fgets(actuator), ' ');
start_force = str2double(start_force(end));

position = [];
force = [];
i1 = 1;

% Specify force or position control : 1 = force, 0 =
   position
% ---------
control = 1;
% ---------

% Wave specifications: Force Control
ampl = 4/0.0155;                % Amplitude : N/0.0155
Fc = 0.5;                       % hertz
offset = 6/0.0155;

SMAC_read_and_set_Force(actuator,0);
tic
% Loop the sine wave
while toc < time
    if control == 0
        % Put your excitation signal here : force
        Pset = ampl * sin(2*pi*Fc*toc) +
           start_position;

        % POSITION CONTROl
```

```
            [raw_pos, raw_force] =
               SMAC_read_and_set_Position(actuator,Pset);

            position(i1) = raw_pos*PperP;
            i1 = i1 + 1;
        else
            % Use this Fset for constant force
            %Fset = 8/0.0155;
            % Put your excitation signal here
            Fset = offset + (ampl * sin(2*pi*Fc*toc));

            % FORCE CONTROl
            if toc > 9 % Offset for mean() reading
                [raw_pos, raw_force] =
                   SMAC_read_and_set_Force(actuator,Fset);

                % Conversion force
                if raw_force <= 100
                    FperP = 0.0153;
                else
                    FperP = 0.0158;
                end
%                 test(i1) = Fset*FperP;

                Fexcitation(i1) = Fset;
                force(i1) = raw_force*FperP;
                t_smac(i1) = toc;
                i1 = i1 + 1;
            end
        end
    end
    % Move back to start_position
    if control == 0
        SMAC_read_and_set_Position(actuator,
           start_position);
    else
        SMAC_read_and_set_Force(actuator,0);

    fclose(actuator)

    save(['data/raw/SMAC/','data_SM',mat2str(counter_smac)
       ,'.mat'])
end
```

Bibliography

[1] "FIT-UP: Functional, individual, tailor-made urogynecological pessary," tech. rep., 12 2021.

[2] C. Lewicky-Gaupp, *Contemporary Use of the Pessary*. Glob. libr. women's med., 2010.

[3] R. Oliver, R. Thakar, and A. H. Sultan, "The history and usage of the vaginal pessary: A review," 12 2011.

[4] CooperSurgical, "Making Life Easier for You and Your Patient."

[5] M. R. Khosravani and T. Reinicke, "3D-printed sensors: Current progress and future challenges," 2 2020.

[6] S. A. Tofail, E. P. Koumoulos, A. Bandyopadhyay, S. Bose, L. O'Donoghue, and C. Charitidis, "Additive manufacturing: scientific and technological challenges, market uptake and opportunities," 1 2018.

[7] Y. Ni, R. Ji, K. Long, T. Bu, K. Chen, and S. Zhuang, "A review of 3D-printed sensors," *Applied Spectroscopy Reviews*, vol. 52, pp. 623–652, 12 2017.

[8] E. Prakken, "Design, modeling, and control of a novel multirotor UAV with embedded 3D-printed thrust force sensor.," tech. rep., 2 2022.

[9] H. Ren, X. Yang, Z. Wang, X. Xu, R. Wang, Q. Ge, and Y. Xiong, "Smart structures with embedded flexible sensors fabricated by fused deposition modeling-based multimaterial 3D printing," *International Journal of Smart and Nano Materials*, 7 2022.

[10] G. Wolterink, P. Dias, R. G. Sanders, F. Muijzer, B. J. van Beijnum, P. Veltink, and G. Krijnen, "Development of soft semg sensing structures using 3d-printing technologies," *Sensors*, vol. 20, pp. 1–19, 11 2020.

[11] S. Zhao, Z. Wang, Y. Lei, J. Zhang, Y. Li, Z. Sun, and Z. Gong, "3D-Printed Soft Pneumatic Robotic Digit Based on Parametric Kinematic Model for Finger Action Mimicking," *Polymers*, vol. 14, 7 2022.

[12] Z. Zhu, H. S. Park, and M. C. McAlphine, "lung printed sensors," *Science Advances*, vol. 6, 6 2020.

[13] M. Schouten, G. Wolterink, A. Dijkshoorn, D. Kosmas, S. Stramigioli, and G. Krijnen, "A Review of Extrusion-Based 3D Printing for the Fabrication of Electro-and Biomechanical Sensors," *IEEE SENSORS JOURNAL*, 8 2020.

[14] J. A. Hernandez, C. Maynard, D. Gonzalez, M. Viz, C. O'Brien, J. Garcia, B. Newell, and T. N. Tallman, "The development and characterization of carbon nanofiber/polylactic acid filament for additively manufactured piezoresistive sensors," *Additive Manufacturing*, vol. 58, 6 2022.

[15] M. Vatani, Y. Lu, E. D. Engeberg, and J. W. Choi, "Combined 3D printing technologies and material for fabrication of tactile sensors," *International Journal of Precision Engineering and Manufacturing*, vol. 16, pp. 1375–1383, 6 2015.

[16] Y. H. Chang, K. Wang, C. Wu, Y. Chen, C. Zhang, and B. Wang, "A facile method for integrating direct-write devices into three-dimensional printed parts," *Smart Materials and Structures*, vol. 24, 6 2015.

[17] "X60 Ultra-Flexible Filament."

[18] Palmiga Innovation, "rubber3dprinting.com."

[19] C. W. Lee and V. F. Nesterenko, "Dynamic deformation of strongly nonlinear toroidal rubber elements," *Journal of Applied Physics*, vol. 114, 8 2013.

[20] J. Zhang and J. Xie, "Investigation of Static and Dynamic Seal Performances of a Rubber O-Ring," *Journal of Tribology*, vol. 140, 7 2018.

[21] P. F. JORDAN, "Stresses and Deformations of the Thin-Walled Pressurized Torus," *Journal of the Aerospace Sciences*, vol. 29, pp. 213–225, 2 1962.

[22] B. Sun, "Small symmetrical deformation of thin torus with circular cross-section," *Thin-Walled Structures*, vol. 163, 6 2021.

[23] T. Piesk, "A torus with a selection of circles on its surface."

[24] I. de Alba Alvarez, "Effect of pessary on the position and orientation of pelvic organs in patients with pelvic organ prolapse (POP)."

[25] F. van Limbeek-van den Noort, "Pessary success mechanisms."

[26] X. Jiang, K. Kim, S. Zhang, J. Johnson, and G. Salazar, "High-temperature piezoelectric sensing," 1 2014.

[27] M. Schouten, B. Prakken, R. Sanders, and G. Krijnen, "Linearisation of a 3D printed flexible tactile sensor based on piezoresistive sensing," *2019 IEEE SENSORS*, pp. 1–4, 2019.

[28] M. Schouten, C. Spaan, D. Kosmas, R. Sanders, and G. Krijnen, "3D printed capacitive shear and normal force sensor using a highly flexible dielectric," in *2021 IEEE Sensors Applications Symposium (SAS)*, (Enschede), University of Twente, IEEE, 9 2021.

[29] A. Aryanfar, M. El Skafi, and W. A. Goddard, "An estimation for the effective force transfer medium in radial loading of the cylindrical and spherical geometries," *Journal of Mechanical Science and Technology*, 12 2022.

[30] NinjaTek, "NinjaFlex-TDS."

[31] "UltiMaker Cura."

[32] Farnell, "SCP03B."

[33] Farnell, "MC002966," 2016.

[34] SMAC-MCA, "SMAC LCA25-050-15F."

[35] OMEGA, "LCMFD-50N Load Cell."

[36] FUTEK, "IAA100 - Voltage Output Load Cell Amplifier."

[37] DEWESoft, "DEWE-43A TECHNICAL REFERENCE MANUAL."

[38] D. Kosmas, "Model-Based Hysteresis Compensation and Control with 3D Printed Lousy Sensors," tech. rep.